Marcinkiewicz–Zygmund inequality and hyperinterpolation on spheres

†based on joint works with Congpei An (Guizhou) and Xiaoming Yuan (Hong Kong)

Hao-Ning Wu
University of Georgia

AMS Spring Eastern Sectional Meeting
Mar 28, 2026

Numerical Integration on Spheres

The Classical Assumption

What numerical analysis assumes

- Exact quadrature rules
- Highly structured point sets
- Full access over sampling locations

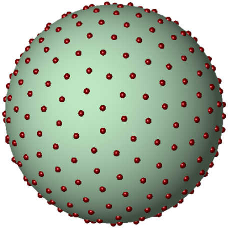

What data gives us

- Scattered or random samples
- Data collected externally
- Limited or no control over point locations

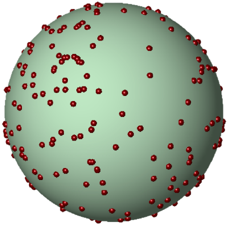

Quadrature exactness is a mathematical luxury, not a practical assumption.

Spherical Designs

❑ Consider spherical integrals

$$\int_{\mathbb{S}^d} f \mathrm{d}\omega = \int_0^{2\pi} \int_{-1}^{1} f(\lambda, \mu) d\mu d\lambda,$$

where $\mathbb{S}^d = \{x \in \mathbb{R}^{d+1} : \|x\|_2 = 1\}$.

latitude: Gauss–Legendre in μ

longitude: uniform grid in λ

✘ Severe point clustering near poles

(a) latitude-longitude grid (b) equal area point

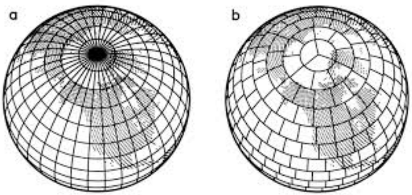

❑ **Spherical analogue of Gauss quadrature**: A spherical t-design $\{x_j\}_{j=1}^{m}$ is a carefully constructed set of points such that

$$\boxed{\frac{1}{|\mathbb{S}^d|} \int_{\mathbb{S}^d} p \mathrm{d}\omega = \frac{1}{m} \sum_{j=1}^{m} p(x_j) \quad \forall p \in \mathbb{P}_t}$$

- High accuracy for approximation, PDEs, and integral equations
- High-accuracy designs are difficult to compute and incompatible with scattered, random, or data-driven sampling.

From Exactness to Marcinkiewicz–Zygmund inequalities

- **Classical View: Accuracy via Exactness**

  Accuracy comes from exact integration:

$$\boxed{\sum_{j=1}^{m} w_j p(x_j) = \int_{\mathbb{S}^d} p \mathrm{d}\omega \quad \forall p \in \mathbb{P}_{2n}}$$

- **Our View: Accuracy via Stability**

  Stability comes from geometric sampling conditions: For $\eta \in [0, 1)$,

$$(1-\eta)\int_{\mathbb{S}^d} p^2 \mathrm{d}\omega \leq \sum_{j=1}^{m} w_j p(x_j)^2 \leq (1+\eta)\int_{\mathbb{S}^d} p^2 \mathrm{d}\omega \quad \forall p \in \mathbb{P}_n,$$

  implying

$$\boxed{\left|\sum_{j=1}^{m} w_j p(x_j)^2 - \int_{\mathbb{S}^d} p^2 \mathrm{d}\omega\right| \leq \eta \int_{\mathbb{S}^d} p^2 \mathrm{d}\omega}$$

We don't need quadrature exactness but MZ.

Why MZ is the right language: Encodes geometry, not exactness

- Includes spherical t-designs as a special case $(\eta = 0 \text{ if } t = 2n)$
- Holds for scattered and random points:

scattered data

(Filbir & Mhaskar, 2011)

- MZ holds if $n \lesssim \eta / h_{\mathcal{X}_m}$

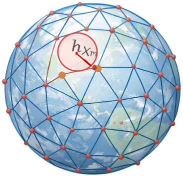

random data

(Le Gia & Mhaskar, 2009)

- MZ holds with probability at least $1 - \bar{c}n^{-\gamma}$ on the condition $m \geq \bar{c}n^d \log n / \eta^2$

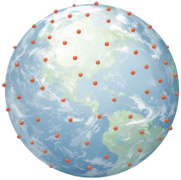

Numerical analysis:
From quadrature exactness-based to MZ-based.

From Numerical Integration to Function Approximation

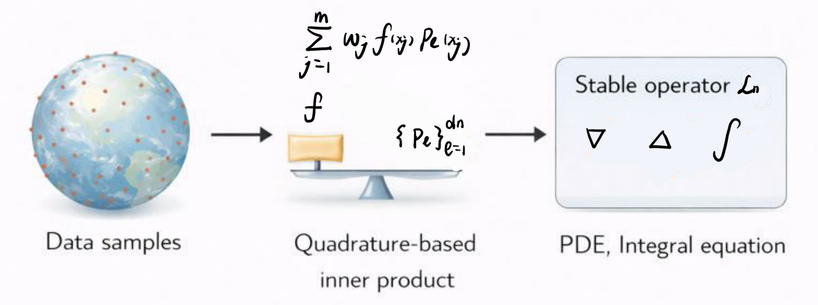

- **Goal**: To build an approximation operator from **sampled data** at scattered locations on the sphere/manifold.
- **Hyperinterpolation**, scheme of approximation: To replace continuous inner products by a **weighted quadrature rule**:

$$\mathcal{L}_n f := \sum_{\ell=1}^{d_n} \langle f, p_\ell \rangle_m p_\ell,$$

where $\langle f, g \rangle_m := \sum_{j=1}^{m} w_j f(x_j) g(x_j)$ with all $w_j > 0$.

What we gain and lose by relaxing exactness

Sloan (1995): quadrature exactness degree $2n$

- $\mathcal{L}_n p = p$ for any $p \in \mathbb{P}_n$
- $\|\mathcal{L}_n f\|_2 \leq |\mathbb{S}^d|^{1/2} \|f\|_\infty$
- $\|\mathcal{L}_n f - f\|_2 \leq 2|\mathbb{S}^d|^{1/2} E_n(f)$

where $E_n(f) := \inf_{p \in \mathbb{P}_n} \|f - p\|_\infty$.

Ours (2022): quadrature exactness degree $n + k$ $(0 < k \leq n)$ + MZ

- $\mathcal{L}_n p = p$ for any $p \in \mathbb{P}_k$
- $\|\mathcal{L}_n f\|_2 \leq \dfrac{|\mathbb{S}^d|^{1/2}}{\sqrt{1-\eta}} \|f\|_\infty$;
- $\|\mathcal{L}_n f - f\|_2 \leq \left(\dfrac{1}{\sqrt{1-\eta}} + 1\right) |\mathbb{S}^d|^{1/2} E_k(f)$

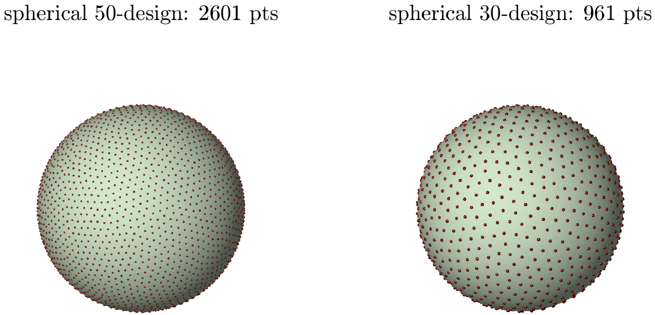

Figure: Spherical 50- and 30-designs, generated by the optimization method proposed by An, Chen, Sloan, and Womersley (2010).

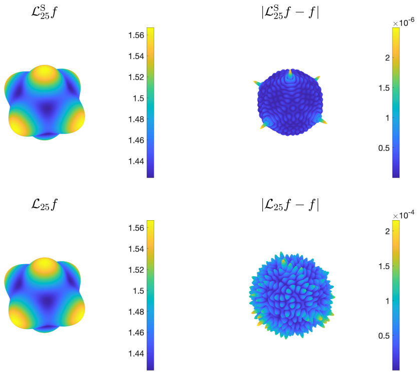

	$n = 25$	
	f: Wendland function (4.3)	
$(k, n+k, m)$	$\\|\mathcal{L}_n f - f\\|_2$	$\\|\mathcal{L}_n f - f\\|_\infty$
(1,26,729)	1.4703e–04	1.1973e–02
(2,27,784)	1.0036e–04	7.2393e–03
(3,28,841)	7.7225e–05	5.6280e–03
(4,29,900)	3.6550e–06	2.2721e–04
(5,30,961)	2.7813e–06	2.1562e–04
(6,31,1024)	9.0144e–07	7.3522e–05
(7,32,1089)	6.3510e–07	5.4311e–05
(8,33,1156)	1.5667e–07	1.4221e–05
(9,34,1225)	1.2137e–07	1.0454e–05
(10,35,1296)	6.0979e–08	7.9442e–06
(11,36,1369)	5.3640e–08	5.4959e–06
(12,37,1444)	1.8896e–08	3.3341e–06
(13,38,1521)	1.9095e–08	3.7055e–06
(14,39,1600)	1.6651e–08	3.2061e–06
(15,40,1681)	1.4991e–08	2.6047e–06
(16,41,1764)	1.4137e–08	2.9486e–06
(17,42,1849)	1.3659e–08	2.5557e–06
(18,43,1936)	1.3509e–08	2.5579e–06
(19,44,2025)	1.3433e–08	2.5896e–06
(20,45,2116)	1.3354e–08	2.6336e–06
(21,46,2209)	1.3318e–08	2.5630e–06
(22,47,2304)	1.3309e–08	2.4906e–06
(23,48,2401)	1.3309e–08	2.5130e–06
(24,49,2500)	1.3294e–08	2.4568e–06
(25,50,2601)	1.3294e–08	2.4959e–06

Accuracy degrades gracefully, not catastrophically.

Computation without Exact Sampling (2024)

Assume the quadrature rule **satisfies the MZ property** only. Then for any $f \in C(\Omega)$:

$$\|\mathcal{L}_n f - f\|_{L^2} \leq \left(\sqrt{1+\eta} \left(\sum_{j=1}^{m} w_j \right)^{1/2} + |\mathbb{S}^d|^{1/2} \right) E_n(f) + \sqrt{\eta^2 + 4\eta} \|p^*\|_{L^2},$$

where $\|f - p^*\|_\infty = E_n(f)$.

- Error bounds depends on sampling geometry
- Applicable to fully data-driven settings

From Approximation to PDEs and Integral Equations

Application I: Semi-linear PDEs on Spheres

- To compute smooth solutions of **semi-linear PDEs** on $\mathbb{S}^{d-1} \subset \mathbb{R}^d$ with dimension $d \geq 3$ of the form

$$u_t = \boldsymbol{L}u + \boldsymbol{N}(u), \quad u(0, x) = u_0(x),$$

where $\boldsymbol{L}$ is a constant-coefficient linear differential operator, and $\boldsymbol{N}$ is a constant-coefficient nonlinear differential (or non-differential) operator of lower order.

  - Nonlinearity + sphere geometry
  - High accuracy traditionally needs highly structured sampling
  - Data-driven point sets break classical assumptions

- Example: **Allen–Cahn equation**

$$u_t = \nu^2 \Delta u - F'(u), \quad u(0, x) = u_0(x),$$

where $F'(u) = f(u) = u^3 - u$.

Our idea: Linearizing the nonlinear part $\boldsymbol{N}(u)$ by hyperinterpolation:

$$\begin{cases} \dfrac{u^{n+1} - u^n}{\tau} = \nu^2 \Delta u^{n+1} - \mathcal{L}_N\left((u^n)^3 - u^n\right), \quad n \geq 0, \\ u^0 = \mathcal{L}_N u_0 \end{cases}$$

where $\tau > 0$ is the time step.

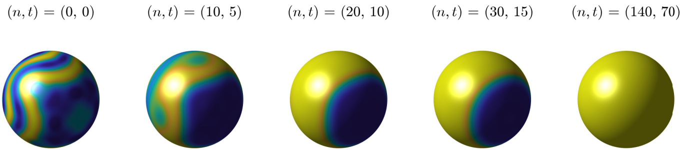

Figure: Numerical solution to the Allen–Cahn equation with $\nu = 0.1$ and initial condition $u(0, x, y, z) = \cos(\cosh(5xz) - 10y)$ using our scheme with $\tau = 0.5$, $N = 15$ and $m = (2N+1)^2 = 961$ **equal area points**

- Consider the Fredholm integral equation of the second kind

$$\varphi(\boldsymbol{x}) - \int_{\mathbb{S}^2} h(|\boldsymbol{x}-\boldsymbol{y}|)K(\boldsymbol{x},\boldsymbol{y})\varphi(\boldsymbol{y})d\omega(\boldsymbol{y}) = f(\boldsymbol{x})$$

on $\mathbb{S}^2$, where $|\boldsymbol{x}-\boldsymbol{y}| := \sqrt{2(1-\boldsymbol{x}\cdot\boldsymbol{y})}$, the kernel K is **continuous** but possibly **oscillatory**, and the weight function $h : (0,\infty) \to \mathbb{R}$ may be **weakly singular**, i.e., h is continuous for all $\boldsymbol{x}, \boldsymbol{y} \in \mathbb{S}^2$ with $\boldsymbol{x} \neq \boldsymbol{y}$, and there exists positive constants M and $\alpha \in (0,2]$ such that

$$|h(|\boldsymbol{x}-\boldsymbol{y}|)| \leq M|\boldsymbol{x}-\boldsymbol{y}|^{\alpha-2};$$

- Potential issues:
  - Singular kernels amplify point clustering
  - Standard pointwise quadrature can explode
  - Need a discretization that respects the singular structure

☞ Let $\{Y_{\ell,k} : \ \ell = 0, \ldots, n, \ \ k = 1, \ldots, 2\ell + 1\}$ be the set of **spherical harmonics** of degree $\leq n$. They are orthogonal polynomials on spheres.

☞ **Modified moments** (derived by Funk–Hecke formula) Computing the singular part analytically

$$\boxed{\int_{\mathbb{S}^2} h(|\boldsymbol{x} - \boldsymbol{y}|) Y_{\ell,k}(\boldsymbol{y}) d\omega(\boldsymbol{y}) = \mu_\ell Y_{\ell,k}(\boldsymbol{x}),}$$

where $\quad (|\boldsymbol{x} - \boldsymbol{y}| := \sqrt{2(1 - \boldsymbol{x} \cdot \boldsymbol{y})}$ and $h(|\boldsymbol{x} - \boldsymbol{y}|) = (2^{1/2}(1 - \boldsymbol{x} \cdot \boldsymbol{y})^{1/2}))$

$$\boxed{\mu_\ell := 2\pi \int_{-1}^{1} h(2^{1/2}(1 - t)^{1/2}) P_\ell(t) dt.}$$

☞ **Example 1:** $h(|\boldsymbol{x}-\boldsymbol{y}|) = |\boldsymbol{x}-\boldsymbol{y}|^{\nu}$ with $-2 < \nu < 0$. Then

$$\boxed{\mu_\ell = 2^{\nu+2}\pi \left(-\frac{\nu}{2}\right)_\ell \frac{\Gamma\left(\frac{\nu+2}{2}\right)}{\Gamma\left(\ell+\frac{\nu}{2}+2\right)}} \text{ with } (x)_n := \frac{\Gamma(x+n)}{\Gamma(x)} \text{ for } x > 0.$$

☞ **Example 2:** $h(|\boldsymbol{x}-\boldsymbol{y}|) = \log|\boldsymbol{x}-\boldsymbol{y}|$. Then

$$\boxed{\mu_\ell = 2\pi \int_{-1}^{1} \log(2^{1/2}(1-t)^{1/2}) P_\ell(t)\,dt} = \pi \int_{-1}^{1} \log(2(1-t)) P_\ell(t)\,dt.$$

☞ **Example 3:** $h(|\boldsymbol{x}-\boldsymbol{y}|) = |\boldsymbol{x}-\boldsymbol{y}|^{\nu_1}|\boldsymbol{x}+\boldsymbol{y}|^{\nu_2}$ with $-2 \le \nu_1, \nu_2 < 0$. Then

$$\boxed{\mu_\ell = 2^{(\nu_1+\nu_2)/2}(2\pi)\int_{-1}^{1}(1-t)^{\nu_1/2}(1+t)^{\nu_2/2}P_\ell(t)\,dt.}$$

A new quadrature rule for the integral operator

For the integral operator $\int_{\mathbb{S}^2} h(|\boldsymbol{x}-\boldsymbol{y}|)K(\boldsymbol{x},\boldsymbol{y})\varphi(\boldsymbol{y})d\omega(\boldsymbol{y})$, we approximate it as

$$
\begin{aligned}
&\int_{\mathbb{S}^2} h(|\boldsymbol{x}-\boldsymbol{y}|)\mathcal{L}_n\left(K(\boldsymbol{x},\cdot)\varphi(\cdot)\right)d\omega(\boldsymbol{y})\\
&= \int_{\mathbb{S}^2} h(|\boldsymbol{x}-\boldsymbol{y}|)\left(\sum_{\ell=0}^{n}\sum_{k=1}^{2\ell+1}\langle K(\boldsymbol{x},\cdot)\varphi, Y_{\ell,k}\rangle_m Y_{\ell,k}(\boldsymbol{y})\right)d\omega(\boldsymbol{y})\\
&= \sum_{\ell=0}^{n}\sum_{k=1}^{2\ell+1}\boxed{\left(\int_{\mathbb{S}^2} h(|\boldsymbol{x}-\boldsymbol{y}|)Y_{\ell,k}(\boldsymbol{y})d\omega(\boldsymbol{y})\right)}\langle K(\boldsymbol{x},\cdot)\varphi, Y_{\ell,k}\rangle_m\\
&= \sum_{j=1}^{m} w_j\left(\sum_{\ell=0}^{n}\sum_{k=1}^{2\ell+1}\boxed{\mu_\ell Y_{\ell,k}(\boldsymbol{x})}Y_{\ell,k}(\boldsymbol{x}_j)\right)K(\boldsymbol{x},\boldsymbol{x}_j)\varphi(\boldsymbol{x}_j)\\
&=: \sum_{j=1}^{m} W_j(\boldsymbol{x})K(\boldsymbol{x},\boldsymbol{x}_j)\varphi(\boldsymbol{x}_j),
\end{aligned}
$$

Two-stage numerical scheme for the integral equation

Let φ_γ denotes the numerical solution:

$$\varphi_\gamma(\boldsymbol{x}) - \sum_{j=1}^{m} W_j(\boldsymbol{x}) K(\boldsymbol{x}, \boldsymbol{x}_j) \varphi_\gamma(\boldsymbol{x}_j) = f(\boldsymbol{x})$$

☞ **First stage** We set $\boldsymbol{x} = \boldsymbol{x}_j$, $j = 1, \ldots, m$, then numerically solves the obtained system of linear equations

$$\varphi_\gamma(\boldsymbol{x}_i) - \sum_{j=1}^{m} W_j(\boldsymbol{x}_i) K(\boldsymbol{x}_i, \boldsymbol{x}_j) \varphi_\gamma(\boldsymbol{x}_j) = f(\boldsymbol{x}_i), \quad i = 1, \ldots, m$$

for the quantities $\varphi_\gamma(\boldsymbol{x}_j)$, $j = 1, \ldots, m$.

☞ **Second stage** The value of $\varphi_\gamma(\boldsymbol{t})$ at any $\boldsymbol{t} \in \mathbb{S}^2$ can be evaluated by the direct usage of

$$\varphi_\gamma(\boldsymbol{t}) = f(\boldsymbol{t}) + \sum_{j=1}^{m} W_j(\boldsymbol{t}) K(\boldsymbol{t}, \boldsymbol{x}_j) \varphi_\gamma(\boldsymbol{x}_j).$$

Toy example setting: Let $\varphi \equiv 1$ and compare the computed solution with 1.
Let $h(\boldsymbol{x}, \boldsymbol{y}) = |\boldsymbol{x} - \boldsymbol{y}|^{-0.5}$ and $K(\boldsymbol{x}, \boldsymbol{y}) = \cos(10|\boldsymbol{x} - \boldsymbol{y}|)$, thus

$$f(\boldsymbol{x}, \boldsymbol{y}) \equiv 1 - 2\pi \int_{-1}^{1} \left(\sqrt{2(1-t)}\right)^{-0.5} \cos\left(10\sqrt{2(1-t)}\right) dt$$
$$\approx \texttt{0.303738699125466}.$$

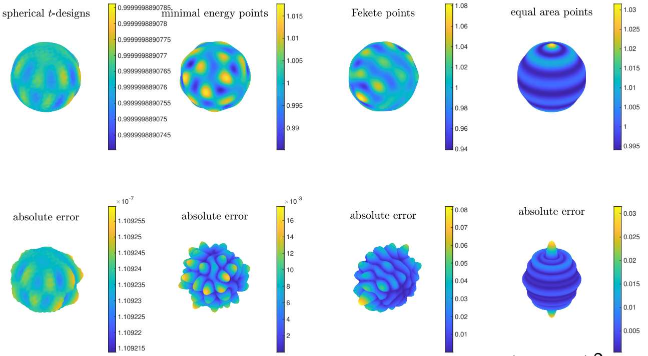

Figure: Numerical solutions with $n = 20$ and $m = (2n+1)^2$.

Thanks for your attention.

Photo taken at the Castillo San Cristóbal, San Juan, Puerto Rico.